RIVER RESEARCH AND APPLICATIONS

River Res. Applic. (2016)

Published online in Wiley Online Library
(wileyonlinelibrary.com) DOI: 10.1002/rra.3113

FLOOD ANALYSIS SUPPORTED BY LOW-COST GEOMETRIC MODELLING

S. ZAZO[a]*, P. RODRÍGUEZ-GONZÁLVEZ[a], J.-L. MOLINA[a], D. HERNÁNDEZ-LÓPEZ[b] AND D. GONZÁLEZ-AGUILERA[a]

[a] *High Polytechnic School of Engineering, University of Salamanca, Hornos Caleros, 50, 05003, Ávila, Spain*
[b] *Institute for Regional Development (IDR), University of Castilla-La Mancha. Campus Universitario s/n, 02071, Albacete, Spain*

ABSTRACT

Today, it is increasingly clear that non-stationarity hydrological and hydraulic variables and processes are occurring largely because of global warming. Accordingly, extreme hydrological events are becoming more common over time, and their effects are creating greater negative impacts on the environment (fluvial geomorphology and floodplains) and society (flood damage). Given this situation, the implementation of adaptation-mitigation measures is vital, as well as an increased knowledge of the interaction between water and physical environments. In the binominal water-terrain, having a reliable digital elevation model (DEM) is essential because of its important influence on fluvial modelling. However, this is frequently a technical-economic problem. The aim of this paper is first to evaluate the compatibility between hydraulics and geometrics for fluvial applications and second to determine the quality of a novel DEM by robust estimators. This was obtained through the photogrammetric processing of digital aerial images acquired from a low-cost camera mounted on an alternative aerial platform. Flood modelling and hydraulic parameters were obtained with the assistance of photogrammetric DEM (mesh size: 0.15 m, vertical accuracy: 0.102 ± 0.081 m, point density: ≈40 point/m^2). Finally, our other goal is to develop a comparative analysis between light detection and ranging and digital photogrammetry on-demand. This comparison revealed that flood modelling by photogrammetric DEM was considerably more detailed than that by light detection and ranging-DEM, mainly because of higher point density and vertical accuracy. Consequently, flood analysis assisted by this novel geometric modelling approach qualifies as a reliable and competitive approach. Copyright © 2016 John Wiley & Sons, Ltd.

KEY WORDS: flood analysis; river geomorphology; fluvial hydraulic; DEM accuracy; structure from motion (SfM); digital photogrammetry on-demand (DPod)

Received 16 July 2016; Revised 11 October 2016; Accepted 27 October 2016

INTRODUCTION

The non-stationarity of hydrological variables due primarily to global warming, together with other factors, is a tangible reality, recognizable even by non-experts. Consequently, hydrological-hydraulic extreme events such as floods, droughts and other events have become more frequent in the water cycle over the last several decades (Huntington, 2006; Labat *et al*., 2004; Lepori *et al*., 2015; Praskievicz, 2016; Reihan *et al*., 2012, Yang *et al*., 2012).

In this sense, global warming causes considerable negative impacts for society, as well as involves considerable environmental, social and economic costs. Furthermore, measures to subvert climate change are having limited effects in the short-medium term, largely attributable to the persistence of anthropogenic effects (IPCC, 2014).

Given this growing global challenge, the implementation of adaptation and/or mitigation measures seems crucial (Poussin *et al*., 2012; Williams *et al*., 2013). Such measures should be addressed not only on the basis of different hydrological scenarios but also via a detailed representation of the physical environment, an essential element for the proper evaluation and management of natural flood risks.

Thus, having reliable and accurate topographic data in a continuous digital elevation model (DEM) form is crucial (Saksena and Merwade, 2015; Wechsler, 2007). Furthermore, it is well known that the accuracy of terrain 3D models is highly dependent on fluvial modelling and hydraulic parameters (Merwade *et al*., 2008, USACE, 2010; Zazo *et al*., 2015). Nevertheless, acquiring DEM data may present a technical-economic problem.

The aim of this paper is to assess the joint behaviour and performance of hydraulics and geometrics, by means of a novel DEM for river applications. This was obtained through the photogrammetric processing of digital aerial images by the structure from motion (SfM) technique. Finally, a comparative analysis of light detection and ranging (LiDAR) technique was performed. A 'pilot test' was carried out via a low-cost passive sensor (digital camera) mounted on a fixed-wing alternative aerial platform. This ultralight motor represented an intermediate solution between aircrafts and unmanned aerial vehicles (Ortega-Terol *et al*., 2014).

*Correspondence to: S. Zazo, High Polytechnic School of Engineering, Salamanca University, Ávila. Area of Hydraulic Engineering. Av. de los Hornos Caleros 50, 05003, Ávila, Spain.
E-mail: szazo@usal.es

Additionally, this paper proposes a method for evaluating the DEM's vertical precision through robust estimators (RE); this method does not require a priori knowledge of errors distribution function (EDF).

Finally, this work demonstrates that digital photogrammetry (DP) can deliver accurate DEMs to analyse the behaviour of fluvial systems on a reliable and competitive basis.

Over the last several decades, geomatic advances have facilitated the development of new instruments and techniques to acquire high-resolution, accurate topographic data. This is mainly due to digital sensors, artificial vision and image processing algorithms. Within the field of river hydraulic and fluvial geomorphology, these advances have substantially transformed 3D ground modelling (Westoby *et al*., 2012). Instruments such as Global Navigation Satellite System (GNSS) and other techniques such as airborne/terrestrial laser scanning are firmly established among researchers (Brasington *et al*., 2000; French, 2003; Hodge *et al*., 2009; Rosser *et al*., 2005). However, they present some limitations. For example, GNSS data have a spatial resolution limited by the operator (Molina *et al*., 2014). Alternatively, airborne laser scanning data entail high operating and logistical costs (Hugenholtz *et al*., 2013; Westoby *et al*., 2012), whereas the terrestrial laser scanning technique is suitable for specific zones but requires a significant investment (Westoby *et al*., 2012), and the data processing is time consuming (Molina *et al*., 2014). A review of current geomatic techniques applied to water resources modelling (with their uncertainties, limitations and spatial resolutions) is available in Molina *et al*. (2014).

On the other hand, artificial/computer vision and novel imagery processing algorithms have revolutionized DP because of the SfM technique (Fonstad *et al*., 2013; Snavely, 2008). Specifically, an object's 3D geometry is reconstructed by 2D images acquired from multiple viewpoints and from various non-calibrated cameras supported by the principle of epipolar geometry (Hartley and Zisserman, 2004). These techniques are extremely useful (Molina *et al*., 2014) and offer maximum time-cost efficiency (Tonkin *et al*., 2014; Zazo *et al*., 2015). However, their highest potential remains in the geomatic products that can be derived, such as dense point clouds, DEMs and orthoimages (Fonstad *et al*., 2013; Tamminga *et al*., 2015).

Additionally, DP creates geomatic products from a unique instrument, a camera (passive sensor). In contrast, the LiDAR technique requires an active sensor to obtain a DEM and a photogrammetric camera that provides an orthoimage.

Currently, alternative aerial platforms [ultra-light motor (ULM), unmanned aerial vehicles (UAV)] based on fixed-wing or multirotor platforms are opening new research doors for the geoscience community (Lejot *et al*., 2007; Westoby *et al*., 2015). Solutions based on fixed-wing platforms are appropriate for flood modelling and fluvial analysis, given their suitability to flight over wide or narrow areas (Ortega-Terol *et al*., 2014; Zazo *et al*., 2015). In contrast, multirotor solutions exhibit an important limitation in autonomy (Hardin and Jensen, 2011) that may negatively impact their applicability to river studies (Ortega-Terol *et al*., 2014).

The growing necessity of producing adequate DEMs for flood modelling (Saksena and Merwade, 2015) is driving the emergence of innovative solutions (time-cost) on the basis of DP on-demand (DPod).

This new research direction towards hybridization between hydraulic and geomatic sciences is characterized by simplicity, quickness and efficiency in the acquisition of topographic data (Molina *et al*., 2014). It also provides efficient and low-cost solutions (Ortega-Terol *et al*., 2014; Tamminga *et al*., 2015; Zazo *et al*., 2015), as well as accurate and detailed topographic products (Tamminga *et al*., 2015; Zazo *et al*., 2015).

MATERIALS

Photogrammetric data

To take full advantage of the potential of new photogrammetry algorithms for the DEM generation, a low-cost digital camera was employed (GoPro Hero 2 model, GoPro, Inc., San Mateo, California, USA). Its main technical characteristics included low weight (167 g) and small dimensions (42 × 60 × 30 mm) suitable for the new generation of fixed-wing UAVs (Toth and Jóźków, 2016). Moreover, the fisheye lens yields a wide field of view of up to 170°, whereas its moderate resolution of 11 megapixels (3840 × 2880) leads to an optimal trade-off for this case study.

According to previous studies in the area (Zazo and Rodríguez-Gonzálvez, 2014; Zazo *et al*., 2015), the planned flight height was established at 200 m above ground level. Flight planning and execution was determined by MFLIP software (Hernandez-Lopez *et al*., 2013).

Light detection and ranging data

Light detection and ranging data are usually applied to flood modelling. In Spain, LiDAR is the geometric base for flood zone mapping (MAGRAMA, 2011). Recently, these data have been provided by the National Plan of Aerial Orthophotography (PNOA, 2016). Here, LiDAR-DEM will be used as ground truthing to evaluate the suitability of DPod-DEM for hydraulic purposes. Table I summarizes the technical characteristics of LiDAR data.

Hydrological data

Water flow data were supplied by the Duero River Basin Authority through a map of instant peak flows under the natural regime (CEDEX, 2013).

Table I. Technical specifications of LiDAR data

Geomatics products		LiDAR data
Point clouds	Spatial resolution. Point density:	0.5 points/m^2
	Average distance between points:	1.41 m
	Vertical precision, RMSE(Z):	±0.20 m
	Maximum error (in 95% of points):	±0.40 m
	Maximum allowable error (Z):	±0.60 m
	Update period (temporal reference)	6 years
Digital elevation model	Mesh size:	1.50 × 1.50 m
Orthoimage	Image resolution:	0.25 m
	Update period (temporal reference):	2 to 3 years

Root mean square rrror, RMSE; LiDAR; light detection and ranging.

Map values were obtained through maximum discharges series, relating the peak flood flow with its annual probability of occurrence (quantile). Through a process of quality and data consistency validation, the gauging of peak flows was adjusted to a distribution function. Frequency adjustment was accomplished through a generalized extreme values function and adjusted by the L-moments method (CEDEX, 2013). Because the point of flow assessment was not a gauging station, a results extrapolation was made for the quantile at that point. This extrapolation was performed according to statistical multiple regression models that relate the quantiles of gauging stations or specific statistics with physiographic and climatic characteristics of the basin. Thus, a quantile can be estimated by these characteristics of the regression.

Methodology

Case Study. The location of the case study was the upper basin of the Adaja River. This subsystem is integrated within the Duero River basin, the largest basin in the Iberian Peninsula (Figure 1a). The area under study (0.50 km^2) is characterized by a meandering fluvial channel with a wide and regular floodplain and a well-defined gravel-bed main channel. It has a length of 1300 m (straight line 1140 m) and according to Martín Vide (2009), a low sinuosity ($s = 1.14$; $1 < s < 1.3$; Figure 1b).

At the morphometric level, the sub-basin of 530 km^2 has a main stream 39.9 km in length, an average height difference of 430 m and a time of concentration of 11.7 h.

Methodology. Our methodology comprises four stages. First, a continuous DEM was built through an image data set acquired from a low-cost digital camera. Then, a complete geometric assessment of this DEM was carried out by means of RE methodology. Subsequently, hydraulic modelling was performed, first via a hydrological model and second via a 1D hydraulic simulation. Finally, as a means of verification, the results (flood modelling and basic hydraulic parameters) were compared with those obtained through more commonly employed DEMs, such as the LiDAR technique (Figure 2).

Stage-1. digital elevation model generation. In this initial stage, DEM was generated by the photogrammetric processing of image data run through Agisoft Photoscan® software. This commercial software is based on the principle of SfM. The objective of this article is not the process itself; however, in depth background on theoretical photogrammetric can be consulted in Snavely (2008), Fonstad *et al.* (2013), Javernick *et al.* (2014), Tonkin *et al.* (2014) and Westoby *et al.* (2012). However, it should be noted that the matching of homologous points among images was performed by the Scale Invariant Feature Transform detector and descriptor (Lowe, 2004).

This processing presents a twofold challenge: 1 the inherent lack of technical details common in black-box solutions for 3D image processing (Cramer *et al.*, 2013; Javernick *et al.*, 2014) and 2 the singular behaviour that a fisheye lens exhibits in a photogrammetric workflow. More specifically, these types of lens have limitations in terms of lens quality and camera shutter. Regarding the former, lens quality is related to variation of interior camera parameters over time. This is solved by the self-calibration protocol of the SfM technique. The latter (camera shutter) determines how light is recorded. Non-professional cameras do not record all light from a scene at the same time, which could cause undesirable effects. To avoid this, flight planning was designed taking into account the platform speed (approximately 11 m·s^{-1}) and a safety ground sample distances (GSD) threshold (5 cm) to compute the minimum necessary exposure time. The images were acquired with a minimum exposure time of 1/800, far from the safety threshold of 1/220 (0.05 m/11 m·s^{-1}).

Empirical experiments lead to the assumption that the employed low-cost camera lens follows a stereographic model. This lens model presents different behaviours than the normal lens, especially between the central point and extremes, because of the great perspective distortion of the lens. Consequently, for a flight height of 200 m, there will be different GSD, ranging from 128 mm at the central point to 300 mm in the extremes. Consequently, to reduce the influence of distortion, it is necessary to consider a specific mathematical distortion model and use masks in the digital images, excluding those excessive GSD points.

The resulting DEM must be geo-referenced: 1 planimetrically with the legal system coordinates of the area, based on

DOI: 10.1002/rra

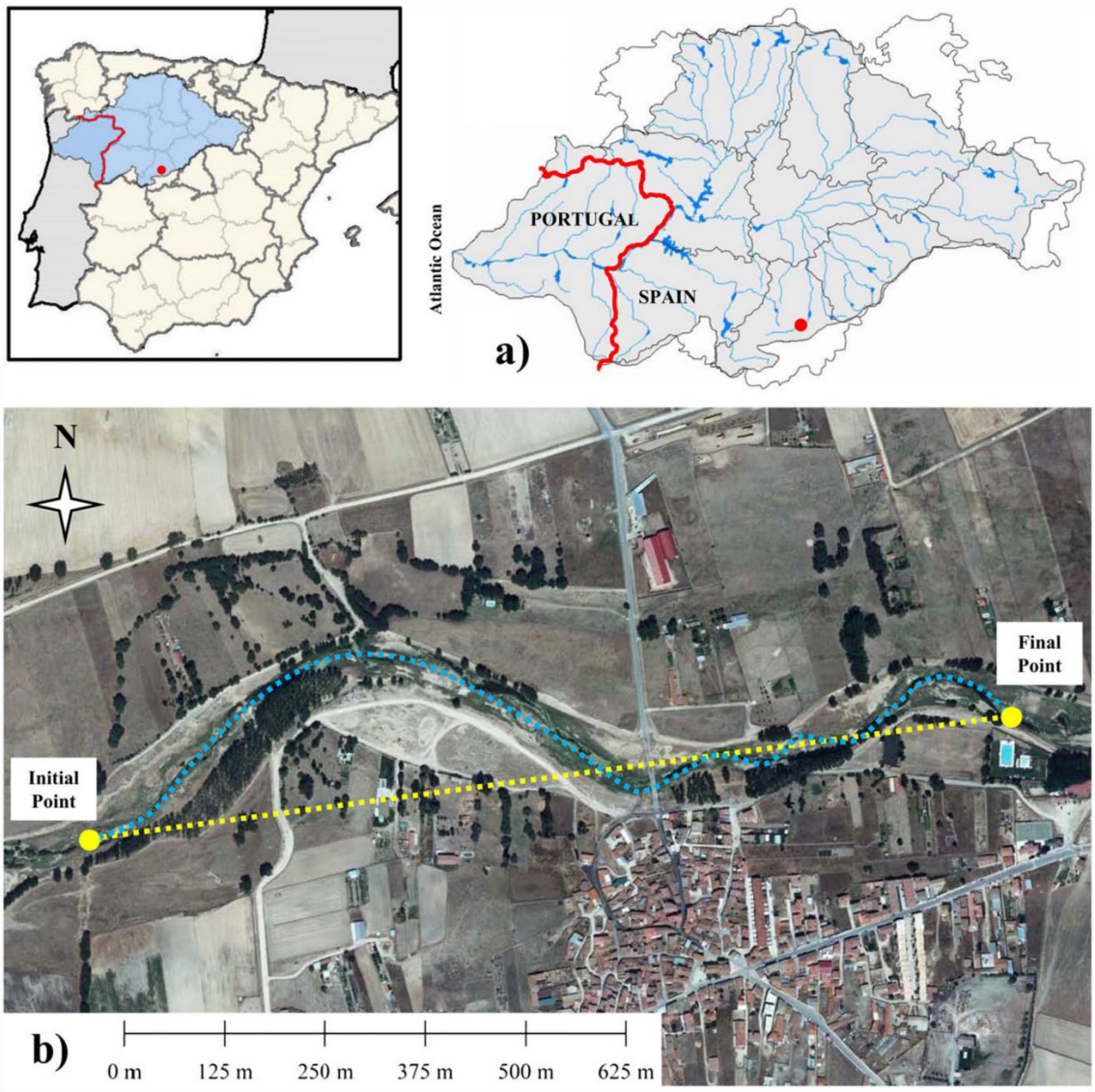

Figure 1. (a) Duero River basin and case study. (b) Studied stretch (Coordinate Reference System: EPSG:25830). [Colour figure can be viewed at wileyonlinelibrary.com]

the following cartographic projection and reference system UTM30N, ETRS89, EPSG:25830 and 2 vertically with the Spanish vertical reference system EPSG:5782. For that, a differential GNSS survey was completed via bi-frequency receiver TRIMBLE R6 as a rover and reference station AVIL (regional GNSS network). The observation method was real–time kinematic. A total of 70 points were observed; 12 ground control points corresponding to artificial targets were used for precise photogrammetric geo-referencing, while the remaining 58 points were used as check points (natural features) for the geometric assessment (Figure 3). Table II shows a summary of the photogrammetric processing, and Table III shows the geomatic products.

Regarding potential problems arising from vegetation, as shown in Hugenholtz *et al.* (2013), Javernick *et al.* (2014) and Lane (2000), they were not relevant to our experiment

DOI: 10.1002/rra

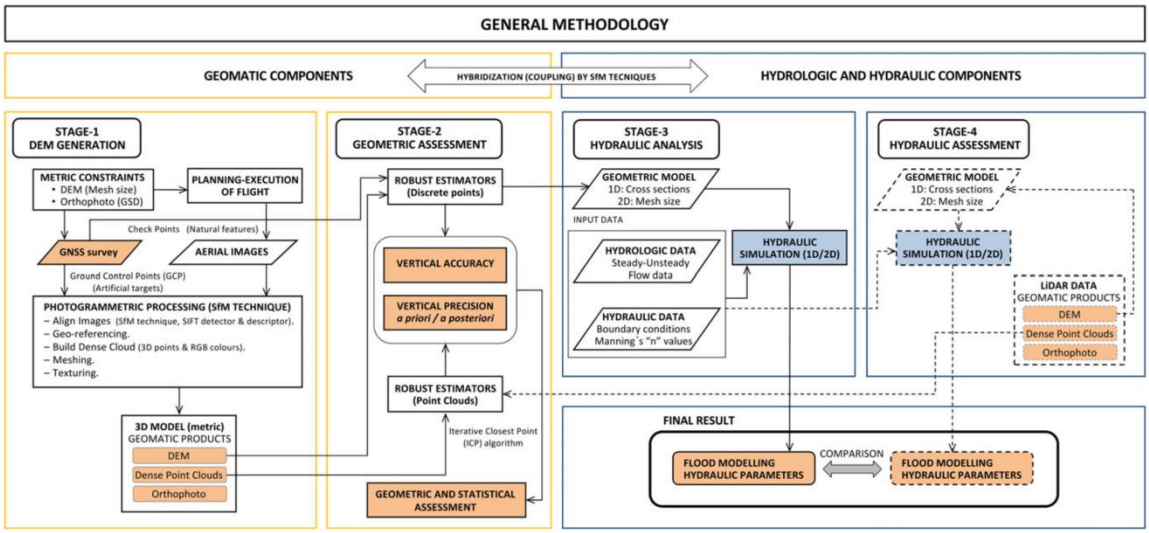

Figure 2. General methodology. [Colour figure can be viewed at wileyonlinelibrary.com]

because the flight execution was carried out according to the phenology of vegetable species in the area. In this way, the influence of vegetation was minimized, allowing the study area to be considered 'vegetation-free'.

In spite of the different substeps involved in photogrammetric DEM generation (images acquisition, GNSS observations, etc.), the final temporal efficiency is optimal for flood analysis tasks. In the first place, image acquisition was carried out at speeds of $11\,m \cdot s^{-1}$, requiring only the displacement of the aerial platform near to the study zone. Secondly, the time required for GNSS observations is directly proportional to the study area extension, which was 2 h in the presented study case. Finally, the processing substep, which can be parallelized and/or subdivided into clusters, was the costliest, requiring 60 h for the case study.

Stage-2. Geometric assessment. The geometric quality of DEM is a fundamental factor for flood modelling because its errors are transmitted entirely to the hydraulic simulation (Bales and Wagner, 2009; Merwade *et al.*, 2008; Wechsler, 2007).

Traditionally, DEM accuracy has been evaluated by mean error, standard deviation, mean absolute error and root mean square error (RMSE) (Hugenholtz *et al.*, 2013; Schwendel *et al.*, 2012, Tamminga *et al.*, 2015). Alternatively, Zazo *et al.* (2015) suggests a metrological approach via an evaluation of the type A uncertainty. However, all of these approaches are characterized by the assumption of a normal distribution of DEM errors.

If EDF does not follow a normal distribution, Gaussian approaches cannot be applied and must be addressed by RE. In this case, the normality assumption was checked by

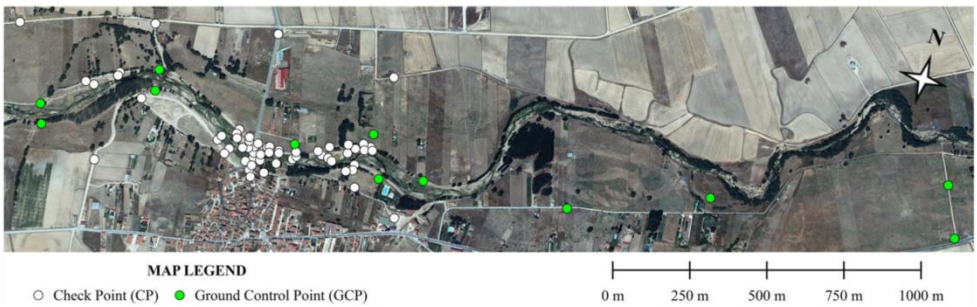

Figure 3. Situation of ground control points (GCP) and check points (CP). [Colour figure can be viewed at wileyonlinelibrary.com]

DOI: 10.1002/rra

Table II. Results of photogrammetric processing

Dataset	Images	1786 (total). Median footprint: 1,340 m^2/image (aprox.)
	Mean executed flight height	187 m
	Average GSD	12.02 cm (orthoimage)
Bundle block adjustment	Matching points	2 394 536 points. Median of 1341 points/image
	Mean reprojection error	0.746 pixels

GSD, ground sample distances.

numerical tests, such as Shapiro–Wilk (Shapiro and Wilk, 1965).

A priori knowledge of EDF is not necessary for RE, an important advantage. Through DEM errors, via a GNSS observation, and in accordance with (Rodriguez-Gonzalvez et *al.*, 2014), it is possible to determine the central tendency and the dispersion of errors through the median (m) and the square root of the BiWeight MidVariance (*BWMV*), respectively. According to Wilcox (1993), *BWMV* is a robust estimator of the statistical dispersion, expressed as

$$BWMV = \frac{j\sum_{i=1}^{j} a_i (x_i - m)^2 \left(1 - U_i^2\right)^4}{\left(\sum_{i=1}^{j} a_i \left(1 - U_i^2\right)\left(1 - 5U_i^2\right)\right)^2} \quad (1)$$

$$U_i = \frac{x_i - m}{9MAD} \quad (2)$$

$$MAD = m(|x_i - m_x|) \quad (3)$$

where j is the number of check points, U is obtained by Equation 2, *MAD* is median absolute deviation (Equation 3), and m_x is the median of the sample data. Lastly, the a parameter could be 0 or 1 depending on the U value. If $-1 \leq U \leq 1$, then a is 1; in any case, a is *0*.

Table III. Characteristics of geomatic products obtained by DPod

Geomatics products		DPod data
Point clouds	Spatial resolution. Point density:	≈40 points/m^2
	Average distance between points:	≈0.15 m
	Vertical precision, by RE(Z):	0.102 ± 0.081 m
	Temporal reference:	Specific (ad hoc)
Digital elevation model	Mesh size:	0.15 × 0.15 m
Orthoimage	Image resolution:	0.12 m
	Temporal reference:	Specific (ad hoc)

DPod, digital photogrammetry on-demand; RE, robust estimators.

It is important to note that this approach by RE over check points (discrete points) could also be applied between point clouds. In this case, one of them would be considered as a reference (LiDAR-DEM) for a direct comparison, as long as they both share the same coordinate system. Alternatively, one could compare points by aligning with the iterative closest point algorithm (Besl and McKay, 1992) to address geo-referencing errors and analyse only the intrinsic geometric cloud errors. The comparison between both point clouds was performed with CloudCompare open source software. Then, the median and *BWMV* were calculated by a custom script.

To contextualize the RE analysis, given that geometric data are provided from two different sources (LiDAR and DPod), the a priori error of the comparison will be expected as

$$e = \pm\sqrt{\left(\sigma_{Z_{LiDAR}}\right)^2 + \left(e_{DPod} \cdot GSD\right)^2} \quad (4)$$

where $\sigma_{Z\ LiDAR}$ is the vertical precision of LiDAR data in metres (PNOA, 2016), e_{DPod} is the reprojection error of bundle block adjustment expressed in pixels and *GSD* is expressed in m/pixel. It is thus possible to obtain a comprehensive comparison, at both the geometric and statistical levels (Figure 2).

Stage-3. Hydraulic analysis. This stage requires the generation of a specific hydraulic model. Based on previous work in this area (Zazo and Rodríguez-Gonzálvez, 2014; Zazo *et al.*, 2015), a water flow corresponding to the 100-year return period (100-YRP) was simulated. For this flow, the floodplain is significantly affected because the carrying capacity of the main channel is significantly exceeded. Additionally, higher return periods do not produce relevant effects on flood modelling because the flood wave undergoes a process of attenuation as a result of the wide and regular floodplain. On the other hand, 100-YRP is a common design flow to describe natural flood risks (Cook and Merwade, 2009).

Steady flow conditions were assumed (Saksena and Merwade, 2015). According to the point of assessment for hydraulic flow (X=351736 m, Y=4497736 m, EPSG: 25830; see Figure . 1b, Final Point) and the map of instant peak flows under the natural regime (CEDEX, 2013), the 100-YRP flow was 229 $m^3 s^{-1}$.

Because during high flow periods, the main channel and floodplain act as a unique channel with no floodplain storage areas and both are totally inundated (Saksena and Merwade, 2015), a 1D flow simulation was carried out with HEC-RAS® software.

Given the strong geomatic component of this research, the following hypotheses were assumed: 1 fixed riverbed

channel, 2 constant flow and 3 the validity of continuity equations and energy between two sections.

Normal hydraulic depth and roughness coefficients (n) were defined as boundary conditions (USACE, 2010). To reflect reality in the study area, the following roughness coefficients were applied: 1 main channel: n from 0.035 to 0.075, 2 floodplain area: n from 0.035 to 0.075 and 0.015 for road. This hydraulic model was calibrated with the Gauge Station Ávila (code number 2046) located downstream of the studied stretch of river.

Stage-4. Hydraulic assessment. Once the previously defined hydraulic simulation was executed, hydrologic and hydraulic parameters were kept fixed. Later, a new hydraulic model was defined, in which DPod-DEM was replaced by LiDAR-DEM (PNOA, 2016). Guided by this approach, the differences in flood analysis and hydraulic outcomes will be exclusively produced by DEMs. Once both hydraulic simulations were completed, the results of basic hydraulic parameters were employed to create flood inundation maps made with a Geographical Information System.

This methodology proves the hydraulic suitability of DPod-DEM. However, it should be noted that this final stage might be optional, depending on LiDAR data availability in the study area. If LiDAR data are not available, DPod-DEM would be carried out exclusively from a geometrical point of view (Stage-2).

Results

Geometric assessment. Firstly, the precision (RMSE(Z)) of GNSS check points was 0.012 ± 0.001 m. Secondly, by these check points, the EDF of DPod-DEM was obtained. Next, the Shapiro–Wilk test was applied to determine whether this EDF followed a Gaussian distribution. The resulting p-value of the hypothesis testing was ≈ 0.005. Because the value achieved was smaller than the signification level ($\alpha = 0.05$), the sample was non-normal. Thus, traditional approaches cannot be applied, and the assessment should be addressed by RE.

From a purely geometric point of view, the REs of the vertical accuracy of DPod-DEM, via 58 discrete points, resulted in a median of 0.102 m and ± 0.081 m as the square root of the *BWMV*. Therefore, the vertical accuracy was (0.102 ± 0.081) m, representing approximately half of the LiDAR-DEM accuracy (± 0.20 m; Table I). In Table III, the main characteristics of geomatic products obtained by the DPod technique are summarized. On the other hand, a complete statistical comparison was performed by point clouds (LiDAR vs DPod). The following ratios should be noted: 0.746 pixel for e_{DPod}, a GSD of 0.12 m/pixel for photogrammetric data and a $RMSE_{(Z)}$ of ± 0.20 m for LiDAR data. Hence according to Equation 4, the a priori error of the comparison, e, was ± 0.219 m.

Applying Equations 1–3 (Stage 2) over 192 097 points, the square root of the *BWMV* was ± 0.169 m. Please note that the comparison was performed at the ground level exclusively, with the goal of detecting differences in the main channel of the river and the floodplain. For that analysis, buildings and vegetation-covered areas were excluded from LiDAR data. Thus, the comparable number of LiDAR points was only 192 097. Figure 4a shows the non-normality of this sample by QQ-plot (as a result of the large amount of points), along with their RE parameters.

Regarding comparisons between point clouds, it is noteworthy that dispersion measures, both a priori (± 0.219 m) and a posteriori (± 0.169 m), show homogeneous values. According to EDF quantiles (Figure 4a), approximately 80% of the errors are within the expected range, with an a priori error interval of [−0.219, +0.219]. Likewise, 95% of the errors belong to the interval [−0.374, +0.343], a range similar to the LiDAR maximum error (± 0.40 m; Table I).

Figure 4b shows the differences between both point clouds, which fell within the expected a priori error interval. Point density and high mesh size resolution of DPod-DEM play a decisive role [Tables I and III; 40 points/m^2 (DPod-DEM) vs 0.5 points/m^2 (LiDAR-DEM), at 0.15×0.15 m (DPod-DEM) vs 1.50×1.50 m (LiDAR-DEM)]. DPod-DEM allows for the in-depth representation of the gravel-bed main channel, as well as the existing masonry walls in the floodplain area (Figure 4b). In fact, the greatest detected discrepancies are associated with these places, as well as in the zone where the bridge is located, because these features were not modelled. In this sense, LiDAR-DEM's resolution does not facilitate the detailed representation of specific zones, such as the thalweg (fluvial geomorphology) and the narrow walls through which the channel flows.

Hydraulic assessment. As previously noted, the last stage of the methodology involves a hydraulic assessment. This was developed through main hydraulic variables obtained from two hydraulic simulations, corresponding to both 3D models considered, LiDAR-DEM and DPod-DEM.

The general flow behaviour is analogous in both cases. Froude number, for the entire cross sections, has similar values ranges [(0.16, 0.65), (0.21, 0.62) to DPod-DEM and LiDAR-DEM, respectively]. The same occurs for average velocity [$(0.51\,m \cdot s^{-1}$, $1.20\,m \cdot s^{-1})$, $(0.61\,m \cdot s^{-1}$, $1.11\,m \cdot s^{-1})$] along all the cross sections (XS1–XS13). Nevertheless, there is a minimal variation in these parameters along the same sections under the two hydraulic simulations (Figure 5a and b).

On the other hand, the variation discovered for the water surface parameter is within the expected geometric interval [−0.374 m, +0.343 m] (see previous section). The mean difference for water surface between both hydraulic simulations was 0.25 m (Figure 5c).

DOI: 10.1002/rra

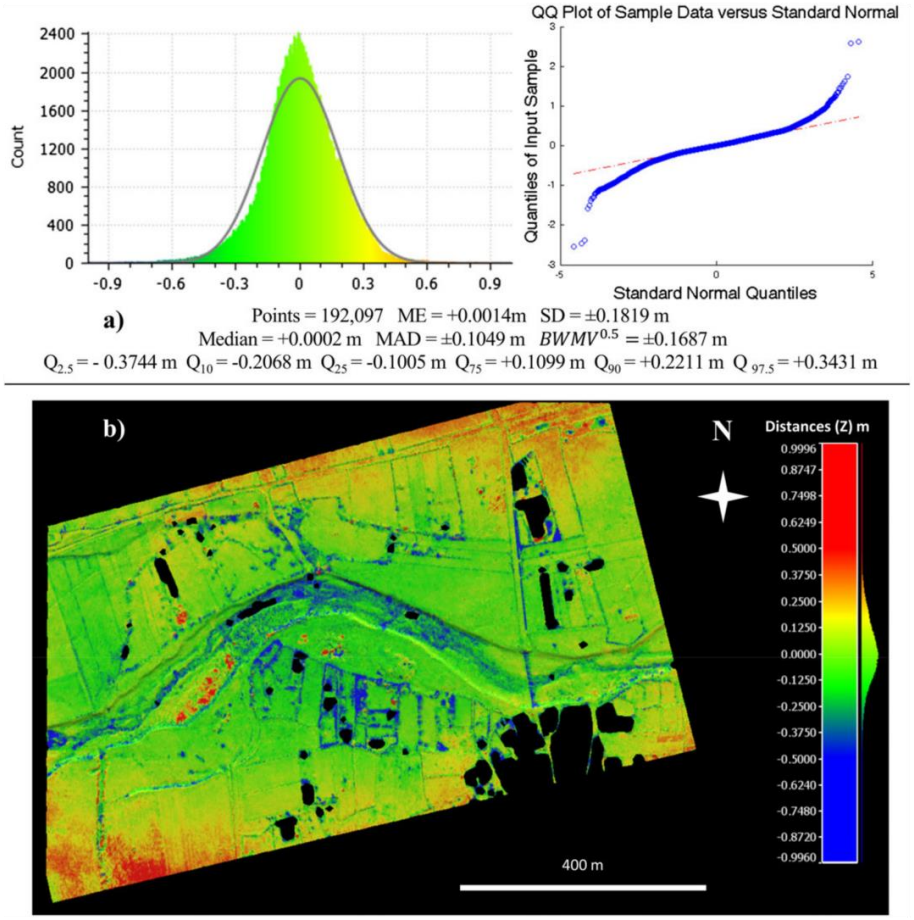

Figure 4. (a) Errors distribution function between point clouds, QQ-plot and quantiles of errors distribution function. (b) Vertical differences between light detection and ranging and digital photogrammetry on-demand data (units: metres) [Colour figure can be viewed at wileyonlinelibrary.com]

In contrast, if LiDAR-DEM results are compared with those obtained by DPod-DEM, there are several noteworthy differences. The average variation is 6.3% for the flow area, 1.8% for the wetted perimeter and 2% for the top width. Furthermore, these differences increase considerably in the case of maximum and minimum values. For flow area (XS12 and XS2), maximum and minimum values were 20% and 8%, respectively. For the wetted perimeter (XS6 and XS5), the maximum and minimum values were 17% and 10%, respectively, and for the top width (XS6 and XS5), the maximum and minimum values were 17% and 10%, respectively, as shown in Figure 5c, d and e. Additionally, these differences could become important in zones without a wide and homogenous floodplain (e.g. urban and peri-urban areas under high anthropogenic pressure due to the existence various elements capable of interacting with flow) and/or in very susceptible floods areas. This might lead to an increased risk and/or uncertainty of flooding. Please note the distinction between risk, defined as the probability that a negative event may happen in the future (always related to events that produce negative or harmful consequences or impacts), and uncertainty, defined as the quantified absence of certainty and typical of hydrological events such as rainfall, runoff or water flow, which are characterized by their highly stochastic nature.

Regarding flooding results, the global differences are not very significant. In fact, the affected and inundated areas vary by only 0.4% (Figure 6a). This is because of the similar floodplain that both DEMs present (Figure 4b) and the resultant attenuation effect. However, the results highlight the positive effect of a higher point density of DPod-DEM over LiDAR-DEM (80 times more), which produces a better

DOI: 10.1002/rra

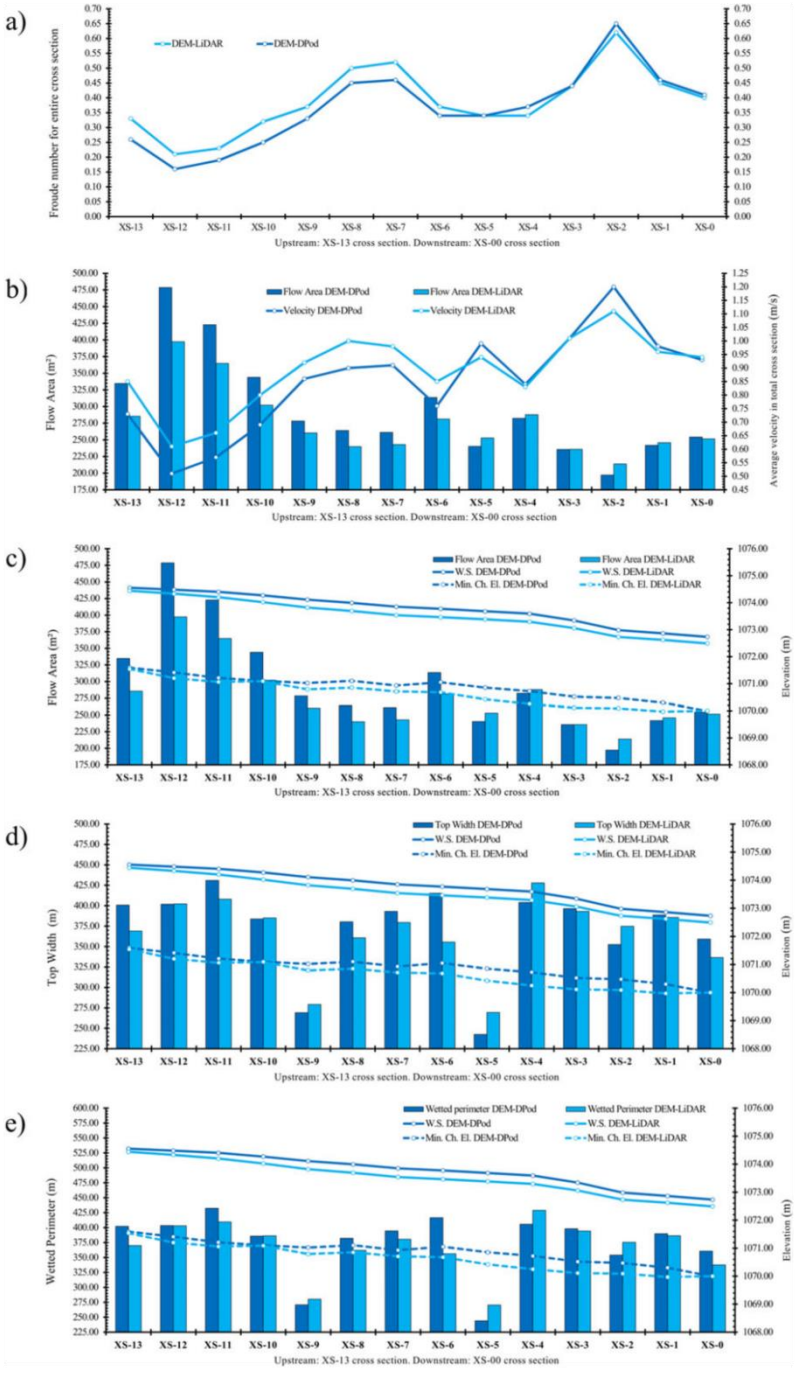

Figure 5. Comparison of 3D models' influence on analysed hydraulic parameters. (a) Froude number. (b) Flow area and average velocity. (c) Flow area and water surface (WS) and minimum channel elevation (Min. Ch. El.). (d) Top width. (e) Top width and WS and Min. Ch. El. (e) Wetted perimeter and WS and Min. Ch. El. Cross section (XS). [Colour figure can be viewed at wileyonlinelibrary.com]

River Res. Applic. (2016)
DOI: 10.1002/rra

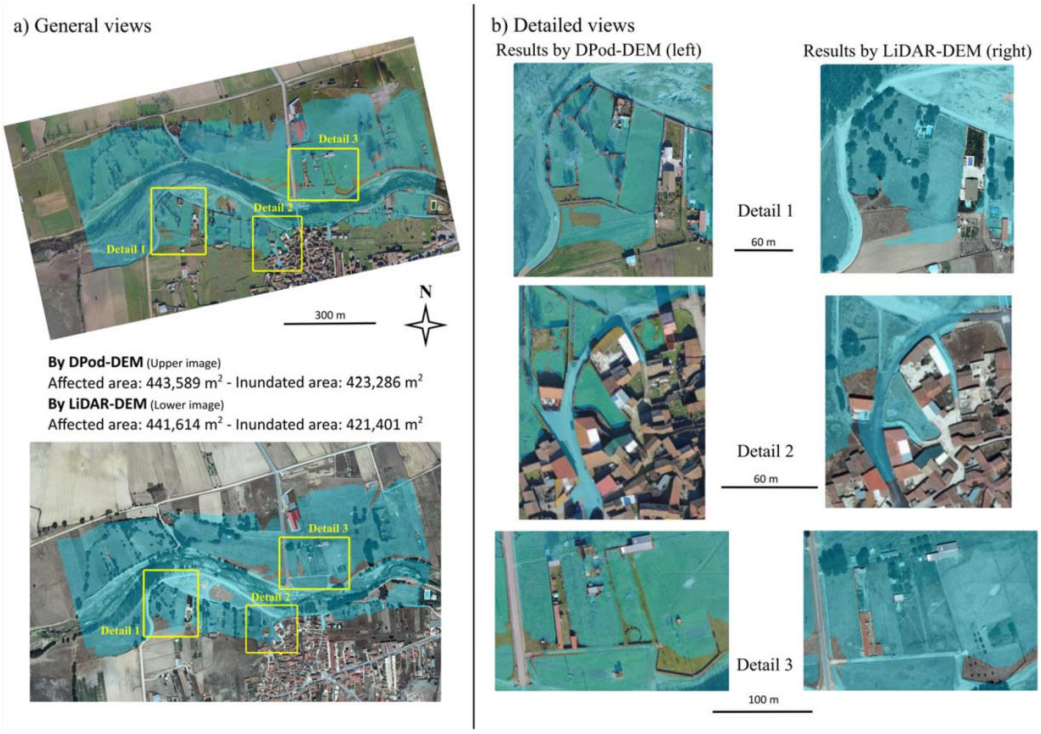

Figure 6. (a) General and (b) detailed view of the flood analysis and influence of point density [Colour figure can be viewed at wileyonlinelibrary.com]

definition of affected and inundated areas. Please note the detailed representation of narrow walls, gates and elements that facilitate the channelling of the flow, especially on the floodplain provided by DPod-DEM (Figure 6b, left images).

DISCUSSION AND CONCLUSIONS

For effective flood analysis, given the inseparable nature of the binominal water-terrain, a reliable DEM is crucial. The proposed photogrammetric 3D model exhibits a vertical accuracy that is double that of LiDAR data (±0.081 vs ±0.20 m) using discrete points. Likewise, in the case of the comparison between point clouds, 95% of errors occur within the interval [−0.374 m, +0.343 m], which is similar to ME (*Z*) LiDAR data (±0.40 m). Furthermore, the geometric assessment (through discrete points and point clouds) showed a similar range of values in relation to their a-priori error estimation.

Regarding hydraulic simulations, at the global level, there were slight variations in basic hydraulic parameters. This is due to the better mesh size achieved by DPod-DEM over LiDAR-DEM as a result of the higher point density and superior vertical accuracy. Consequently, DPod-DEMs applied to other fluvial systems could facilitate the performance of more accurate natural flood risk assessment and knowledge of flow than LiDAR-DEMs.

On the other hand, the higher point density obtained by DPod (40 points/m^2) versus LiDAR (0.50 points/m^2) has provided a more detailed representation of the terrain. If it is expressed as mesh size, 0.15 × 0.15 m vs 1.50 × 1.50 m, this means that DPod-DEM has 10 times more spatial resolution than LiDAR-DEM. At the fluvial geomorphology level, this spatial resolution could detect changes within specific areas, such as the thalweg, as well as increase the knowledge of flow on the floodplain. Mesh size achieved and findings obtained could be useful for the multitemporal analysis of riverbed changes and developing 2D/3D hydraulic models.

Digital photogrammetry on-demand has provided updated data, ad hoc, without a time lag. Because of the intrinsic versatility of flights, narrow and linear areas could be recorded and analysed, representing a suitable solution for river applications. Future research should focus on the application of this technique to determine the optimal relationship between the point density of DEMs and vertical accuracy in terms of hydrological data precision. This will result in knowing the

DOI: 10.1002/rra

final precision of the hydraulic simulation, taking into account the accuracy that the hydraulic model can offer.

There was a reasonable geometric and statistical compatibility among both DEMs (photogrammetric versus LiDAR). However, because spatial resolutions (0.15 m vs 1.41 m) and vertical accuracies (0.081 m vs 0.20 m) are different, they should be taken into account if one wants to integrate both products (LiDAR and photogrammetric) in a continuous DEM. Regarding the photogrammetric technique, it should be noted that via a GSD control, it is possible to scale the geomatic products, by different flight heights or platforms (ULM and UAV based on fixed-wing or multirotor). Accordingly, a lower flight height could possibly obtain superior spatial resolution and thus higher point density and vertical accuracy, as well as a higher processing time, because of the increased number of images. Moreover, the low weight of tested sensor makes it compatible to use on board fixed-wing or multirotor UAV types.

A methodology is also proposed for evaluating the DEM vertical accuracy by RE, which can be applied without a priori knowledge of EDF over any geometric error sample.

This paper has demonstrated that DPod can be considered: 1 an accurate, reliable and cost effective tool to analyse the behaviour of fluvial systems, 2 a suitable technique in places where LiDAR data are not available or where high quality topographic data are unavailable and 3 an effective complement to common flood analysis techniques, such as LiDAR or classic topography.

Regarding future research, the authors plan to investigate the variability of river bed channel monitoring based on river bed channel geometry as well as add the new understanding of riverbed geometry to simulated hydraulic models. Consequently, geometric dynamics could be discerned and incorporated via this methodology, resulting in a recalculation of the hydraulic behaviour of the system.

ACKNOWLEDGEMENTS

Authors thank especially the Institute for Regional Development of University of Castilla-La Mancha for the equipment made available for this work (MultiSpectral Airborne System (MUSAS) and ULM flight platform); and Mr Diego Guerrero Sevilla for the execution of the flight.

This research has been partially supported by the GESINH-IMPADAPT project (CGL2013-48424-C2-2-R) of the Spanish Ministry of Economy and Competitiveness (Plan Estatal I+C+T+I 2013–2016).

REFERENCES

Bales JD, Wagner CR. 2009. Sources of uncertainty in flood inundation maps. *Journal of Flood Risk Management* **2**: 139–147.

Besl PJ, Mckay ND. 1992. A method for registration of 3-D shapes. *IEEE Transactions on Pattern Analysis and Machine Intelligence* **14**: 239–256.

Brasington J, Rumsby BT, Mcvey RA. 2000. Monitoring and modelling morphological change in a braided gravel-bed river using high resolution GPS-based survey. *Earth Surface Processes and Landforms* **25**: 973–990.

CEDEX. 2013. Mapa de caudales máximos instantáneos en régimen natural asociados a distintos periodos de retorno. *CAUMAX*.

Cook A, Merwade V. 2009. Effect of topographic data, geometric configuration and modeling approach on flood inundation mapping. *Journal of Hydrology* **377**: 131–142.

Cramer M, Haala N, Rothermel M, Leinss B, Fritsch D. 2013. UAV@LGL - Pilot Study of the Use of UAV for National Mapping in Germany. *Photogrammetrie Fernerkundung Geoinformation*: 495–509.

Fonstad MA, Dietrich JT, Courville BC, Jensen JL, Carbonneau PE. 2013. Topographic structure from motion: a new development in photogrammetric measurement. *Earth Surface Processes and Landforms* **38**: 421–430.

French JR. 2003. Airborne LiDAR in support of geomorphological and hydraulic modelling. *Earth Surface Processes and Landforms* **28**: 321–335.

Hardin PJ, Jensen RR. 2011. Small-scale unmanned aerial vehicles in environmental remote sensing: challenges and opportunities. *Giscience & Remote Sensing* **48**: 99–111.

Hartley R, Zisserman A. 2004. *Multiple View Geometry in Computer Vision*. Cambridge University Press: London.

Hernandez-Lopez D, Felipe-Garcia B, Gonzalez-Aguilera D, Arias-Perez B. 2013. An automatic approach to UAV flight planning and control for photogrammetric applications: a test case in the Asturias region (Spain). *Photogrammetric Engineering and Remote Sensing* **79**: 87–98.

Hodge R, Brasington J, Richards K. 2009. Analysing laser-scanned digital terrain models of gravel bed surfaces: linking morphology to sediment transport processes and hydraulics. *Sedimentology* **56**: 2024–2043.

Hugenholtz CH, Whitehead K, Brown OW, Barchyn TE, Moorman BJ, LeClair A, Riddell K, Hamilton T. 2013. Geomorphological mapping with a small unmanned aircraft system (sUAS): Feature detection and accuracy assessment of a photogrammetrically-derived digital terrain model. *Geomorphology* **194**: 16–24.

Huntington TG. 2006. Evidence for intensification of the global water cycle: review and synthesis. *Journal of Hydrology* **319**: 83–95.

IPCC. 2014. Intergovernmental panel on climate change. Fifth Assessment Report (AR5) http://www.ipcc.ch (accessed 03/01/2016).

Javernick L, Brasington J, Caruso B. 2014. Modeling the topography of shallow braided rivers using structure-from-motion photogrammetry. *Geomorphology* **213**: 166–182.

Labat D, Godderis Y, Probst JL, Guyot JL. 2004. Evidence for global runoff increase related to climate warming. *Advances in Water Resources* **27**: 631–642.

Lane SN. 2000. The measurement of river channel morphology using digital photogrammetry. *Photogrammetric Record* **16**: 937–957.

Lejot J, Delacourt C, Piegay H, Fournier T, Tremelo M, Allemand P. 2007. Very high spatial resolution imagery for channel bathymetry and topography from an unmanned mapping controlled platform. *Earth Surface Processes and Landforms* **32**: 1705–1725.

Lepori F, Pozzoni M, Pera S. 2015. What drives warming trends in streams? A case study from the alpine foothills. *River Research and Applications* **31**: 663–675.

Lowe DG. 2004. Distinctive image features from scale-invariant keypoints. *International Journal of Computer Vision* **60**: 91–110.

MAGRAMA. 2011. *Guía Metodológica para el desarrollo del Sistema Nacional de Cartografía de Zonas Inundables*. Ministerio de Agricultura, Alimentación y Medio Ambiente. Gobierno de España: Madrid.

Martín Vide JP. 2009. Nociones de morfología fluvial. *Ingeniería de ríos*: 27–30.

Merwade V, Olivera F, Arabi M, Edleman S. 2008. Uncertainty in flood inundation mapping: current issues and future directions. *Journal of Hydrologic Engineering* **13**: 608–620.

DOI: 10.1002/rra

Molina JL, Rodriguez-Gonzalvez P, Carmen Molina M, Gonzalez-Aguilera D, Espejo F. 2014. Geomatic methods at the service of water resources modelling. *Journal of Hydrology* **509**: 150–162.

Ortega-Terol D, Moreno MA, Hernandez-Lopez D, Rodriguez-Gonzalvez P. 2014. Survey and classification of large woody debris (LWD) in streams using generated low-cost geomatic products. *Remote Sensing* **6**: 11770–11790.

PNOA. 2016. http://pnoa.ign.es/ (accessed 11/11/2015).

Poussin JK, Bubeck P, Aerts JCJH, Ward PJ. 2012. Potential of semi-structural and non-structural adaptation strategies to reduce future flood risk: case study for the Meuse. *Natural Hazards and Earth System Sciences* **12**: 3455–3471.

Praskievicz S. 2016. Impacts of projected climate changes on streamflow and sediment transport for three snowmelt-dominated rivers in the interior Pacific Northwest. *River Research and Applications* **32**: 4–17.

Reihan A, Kriauciuniene J, Meilutyte-Barauskiene D, Kolcova T. 2012. Temporal variation of spring flood in rivers of the Baltic States. *Hydrology Research* **43**: 301–314.

Rodriguez-Gonzalvez P, Garcia-Gago J, Gomez-Lahoz J, Gonzalez-Aguilera D. 2014. Confronting passive and active sensors with non-Gaussian statistics. *Sensors* **14**: 13759–13777.

Rosser NJ, Petley DN, Lim M, Dunning SA, Allison RJ. 2005. Terrestrial laser scanning for monitoring the process of hard rock coastal cliff erosion. *Quarterly Journal of Engineering Geology and Hydrogeology* **38**: 363–375.

Saksena S, Merwade V. 2015. Incorporating the effect of DEM resolution and accuracy for improved flood inundation mapping. *Journal of Hydrology* **530**: 180–194.

Schwendel AC, Fuller IC, Death RG. 2012. Assessing DEM interpolation methods for effective representation of upland stream morphology for rapid appraisal of bed stability. *River Research and Applications* **28**: 567–584.

Shapiro SS, Wilk MB. 1965. An analysis of variance test for normality (complete samples). *Biometrika* **52**: 591–611.

Snavely N. 2008. *Scene Reconstruction and Visualization from Internet Photo Collections*. PhD thesis, University of Washington: USA.

Tamminga A, Hugenholtz C, Eaton B, Lapointe M. 2015. Hyperspatial remote sensing of channel reach morphology and hydraulic fish habitat using an unmanned aerial vehicle (UAV): a first assessment in the context of river research and management. *River Research and Applications* **31**: 379–391.

Toth C, Jóźków G. 2016. Remote sensing platforms and sensors: a survey. *ISPRS Journal of Photogrammetry and Remote Sensing* **115**: 22–36.

Tonkin TN, Midgley NG, Graham DJ, Labadz JC. 2014. The potential of small unmanned aircraft systems and structure-from-motion for topographic surveys: a test of emerging integrated approaches at Cwm Idwal, North Wales. *Geomorphology* **226**: 35–43.

USACE. 2010. *HEC-RAS*. River Analysis System Hydraulic: Hydraulic Reference Manual.

Wechsler SP. 2007. Uncertainties associated with digital elevation models for hydrologic applications: a review. *Hydrology and Earth System Sciences* **11**: 1481–1500.

Westoby MJ, Brasington J, Glasser NF, Hambrey MJ, Reynolds JM. 2012. 'Structure-from-Motion' photogrammetry: A low-cost, effective tool for geoscience applications. *Geomorphology* **179**: 300–314.

Westoby MJ, Dunning SA, Woodward J, Hein AS, Marrero SM, Winter K, Sugden DE. 2015. Sedimentological characterization of antarctic moraines using UAVS and structure-from-motion photogrammetry. *Journal of Glaciology* **61**: 1088–1102.

Wilcox RR. 1993. Comparing the biweight midvariances of 2 independent groups. *Statistician* **42**: 29–35.

Williams K, Gupta R, Hopkins D, Gregg M, Payne C, Joynt JLR, Smith I, Bates-Brkljac N. 2013. Retrofitting England's suburbs to adapt to climate change. *Building Research and Information* **41**: 517–531.

Yang C, Yu Z, Hao Z, Zhang J, Zhu J. 2012. Impact of climate change on flood and drought events in Huaihe River Basin, China. *Hydrology Research* **43**: 14–22.

Zazo S, Rodríguez-Gonzálvez P. 2014. Estudio de la aplicación de la tecnología de aeronaves ultraligeras motorizadas (tipo ULMs), de coste reducido y baja altura de vuelo, en vuelos fotogramétricos de detalle, para Estudios y Proyectos Hidráulicos y/o de Ingeniería Fluvial. Tesis Fin de Máster.Universidades de Salamanca y Valladolid.

Zazo S, Molina J, Rodriguez-Gonzalvez P. 2015. Analysis of flood modeling through innovative geomatic methods. *Journal of Hydrology* **524**: 522–537.